# Stability and Reliability of Enhanced External-Internal Motion Correlation via Dynamic Phase-Shift Corrections Over 30-min Timeframe for Respiratory-Gated Radiotherapy

Andrew Milewski, MD, PhD[1], and Guang Li, PhD[1] 🄳

## Abstract

To assess the stability of patient-specific phase shifts between external- and internal-respiratory motion waveforms, the reliability of enhanced external–internal correlation with phase-shift correction, and the feasibility of guiding respiratory-gated radiotherapy (RGRT) over 30 min. In this clinical feasibility investigation, external bellows and internal-navigator waveforms were simultaneously and prospectively acquired along with two four-dimensional magnetic resonance imaging (4DMRI) scans (6–15 m each) with 15–20 m intervals in 10 volunteers. A bellows was placed 5 cm inferior to the xiphoid to monitor abdominal motion, and an MR navigator was used to track the diaphragmatic motion. The mean phase-domain (MPD) method was applied, which combines three individual phase-calculating methods: phase-space oval fitting, principal component analysis, and analytic signal analysis, weighted by the reciprocal of their residual errors (RE) excluding outliers (RE >2σ). The time-domain cross-correlation (TCC) analysis was applied for comparison. Dynamic phase-shift correction was performed based on the phase shift detected on the fly within two 10 s moving datasets. Simulating bellows-triggered gating, the median and 95% confidence interval for the navigator's position at beam-on/beam-off and %harm (percentage of beam-on time outside the safety margin) were calculated. Averaged across all subjects, the mean phase shifts are found indistinguishable ($p > .05$) between scan 1 ($55° \pm 9°$) and scan 2 ($59° \pm 11°$). Using the MPD method the averaged correlation increases from $0.56 \pm 0.22$ to $0.85 \pm 0.11$ for scan 1 and from $0.47 \pm 0.30$ to $0.84 \pm 0.08$ for scan 2. The TCC correction results in similar results. After phase-shift correction, the number of cases that were suitable for amplitude gating (with <10%harm) increased from 2 to 17 out of 20 cases. A patient-specific, stable phase-shift between the external and internal motions was observed and corrected using the MPD and TCC methods, producing long-lasting enhanced motion correlation over 30m. Phase-shift correction offers a feasible strategy for improving the accuracy of tumor-motion prediction during RGRT.

## Keywords

## Introduction

Respiratory-induced tumor motion is one of the largest sources of uncertainties in radiation therapy of a mobile tumor, such as lung cancer, and a large motion margin must be applied to overcome the motion uncertainty. The motion safety margin enlarges the treatment target volume multifold from the clinical tumor volume (CTV) to the internal tumor volume (ITV), defined as the motion envelope of the CTV (ICRU, 2010).[1] Because the ITV encompasses a large volume of healthy tissue, a lowered radiation dose is often prescribed and delivered to the tumor to

avoid exceeding the tolerable toxicity of nearby organs at risk (OARs), including the central lung region with serial functionality, the so-called "no-fly-zone."[2] To reduce the motion margin,

---

[1] Department of Medical Physics, Memorial Sloan Kettering Cancer Center, New York, NY, USA

**Corresponding Author:**
George (Guang) Li, PhD, DABR, Attending Physicist, Department of Medical Physics, Memorial Sloan Kettering Cancer Center, New York, NY, USA.
Email: lig2@mskcc.org

various methods have been proposed, developed, and applied in the clinic, including breath-holding, respiratory gating, and tumor tracking.[3–7] Several approaches, including the CyberKnife LINAC (linear accelerator) system, rely on fluoroscopy or frequent radiographic imaging coupled with a real-time tumor-motion prediction model and an external surrogate.[8–10] The Calypso system using electromagnetic transponders,[7,11,12] and, more recently, the MR-integrated LINAC (MRL) system using 2D cine MR[13–15] have been applied clinically, but implanting the Calypso transponder(s) precludes the possibility of follow-up MR imaging at the disease site and the MRL may yet require substantial investment and resources. Therefore, applying real-time optical imaging (or external surrogates) together with an external-to-internal motion prediction model and periodic radiographic verification remains a viable clinical option in the majority of conventional iso-centric LINACs for respiratory-gated radiotherapy (RGRT).

Although various external–internal motion prediction models have been reported, such as a 5D model,[16] deformation models,[17,18] a biomechanical model,[19] a semi-physical sprint-dashpot model,[20] a physical motion perturbation model,[21] and machine-learning models,[22,23] only correlation-based models have been applied clinically for real-time, image-guided radiotherapy (IGRT). To apply a correlation-based prediction model, a patient should demonstrate a high external–internal motion correlation at the simulation using fiducial markers that are implanted close to the tumor.[24] Marker-less approaches that simplify the clinical procedure and avoid any implant complications have also been studied,[8,25,26] and some of these strategies have been implemented in radiotherapy clinics.[27] Even if the motion correlation is high, the correlation model must be periodically verified and updated with radiographic imaging to accommodate changes in the patient's breathing behavior, which often necessitates rebuilding the predictive model and prolonging treatment.[28]

The quality of the external–internal motion correlation is significantly affected by the phase shift between the external- and internal-motion waveforms.[29–31] Large patient-specific phase shifts may deteriorate the correlation between the two waveforms. We previously developed a phase-domain approach to detect the phase shifts between the external-bellows and internal-navigator waveforms acquired simultaneously during a 4DMRI scan, and we evaluated whether the correlation can be enhanced by correcting the phase shift.[32] However, the duration of the 4DMRI scans was shorter than a radiotherapy treatment, necessitating an assessment of the stability and reliability of phase shifts and enhanced correlations over timeframes that are relevant for radiotherapy treatments. That different external surrogates may disagree in their predictions of a tumor's position raises additional concerns about the accuracy of tumor-position prediction by the correlative strategies employed in RGRT.[33] Due to the uncertainty in correlative prediction, x-ray imaging is often required to verify the tumor's position when the radiation beam is turned on or off.[31,34]

In this study, we employed two sets of 4DMRI scans (6–15 m) separated by a 15–20 m gap in 10 healthy volunteers under an IRB-approved protocol. The external motion was detected using a bellows system and the internal motion was measured concurrently from the diaphragm's motion detected by an MR navigator during 4DMRI scans. The dynamically detected phase-shift and enhanced correlation were evaluated within each scan and compared between the two scans. We also examined whether correcting the phase shift improves the quality of amplitude-triggered respiratory gating. We evaluated a theoretical tumor's position at beam-on/beam-off times and we simulated the percentage of time (%harm) that radiation would be delivered outside of a safety margin.

## Methods

In this clinical feasibility investigation study, volunteer subjects' data were acquired under clinical conditions and employed to assess the stability of patient-specific phase shift, reliability of the enhancement of external–internal motion correlation, and feasibility of applying the phase-shift correction technique to improve RGRT.

### Concurrent External and Internal Waveforms Acquired During Multiple 4DMRI Scans

Motion waveforms from the external bellows (at 496 Hz) and the internal navigator (at 20 Hz) were acquired concurrently and prospectively during two respiratory-correlated 4DMRI scans using a 3T MR scanner (Ingenia, Philips Healthcare, Amsterdam, Netherland) in 10 healthy volunteers under an IRB-approved protocol. The bellows was placed 5 cm inferior to the sternum's xiphoid process and the navigator ($3 \times 3 \times 6$ cm$^3$) was configured at the dome of the right diaphragm. The first 4DMRI scan was in the coronal direction and the second scan was in the sagittal direction. Depending on breathing irregularities, a 4DMRI scan lasted 6–15 min, and the second scan started 15–20 min after the first scan ended. The navigator signal was continuous except at times when 2D coronal-or sagittal-slice images were acquired for the reconstruction of 4DMRI.[35] The bellows signal was continuous, not interrupted by MR acquisition. Because both waveforms were acquired concurrently on the fly prospectively during the 4DMRI scans, they represented the motion of the respiratory organ in real time.

The initial timestamps (in milliseconds) in the log files of the scanner and bellows systems were used to synchronize the navigator and bellows waveforms. To assess the phase shift, an automated algorithm identified navigator-waveform segments containing holes no longer than 0.3 s, and the small gaps (up to 0.3 s) were filled in by linear interpolation. Corresponding time segments from the bellows signal were extracted and downsampled to match the 20 Hz frequency of the navigator.

To assess the phase shift, all available pairs of navigator and bellows time segments throughout a scan were divided into 10-s sampling windows. When the length of a time segment permitted multiple sampling windows, each 10-s sampling window overlapped with 5 s of the subsequent window.

In phase space, the occurrence of ellipsoidal trajectories (navigator vs. bellows) confirmed the existence of a phase shift between the two waveforms.[29,32] Estimates of the phase shift were obtained via phase-space oval fitting (POF), principal component analysis (PCA), and analytic signal analysis (ASA) methods. These results were combined as the mean phase-domain (MPD) method (described below). After correcting the calculated phase shift, the resulting correlation between the two waveforms was compared with the original correlation and with the maximum value of the time-domain cross-correlation (TCC) (Figure 1).

## MPD Method

A combination of three phase-domain methods (POF, PCA, and ASA) was developed and published previously as the MPD method[32] and re-implemented in MATLAB (Version 2020a) to allow automatic data sampling for dynamically estimating the phase shift. Automating the data-sampling strategy significantly reduced data-processing times; the updated algorithm can readily be applied for real-time, online data processing in future clinical applications. When a phase shift was calculated using the three methods, their residual errors (RE) were also estimated and used to calculate the weighting factor (reciprocal of RE) in the MPD method, as shown in Equation 1.

$$\phi^{MPD}(t) = \frac{[w^{POF}\phi^{POF} + w^{PCA} + \phi^{PCA} + w^{ASA}\phi^{ASA}]}{2[w^{POF} + w^{PCA} + w^{ASA}]}$$
$$+ \frac{1}{2}\phi^{MPD}(t-1), \tag{1}$$

$$w^i = \frac{1}{RE^i}, \quad \text{if } \phi^i < 2\sigma; i = POF, PCA, \text{ or } ASA \tag{1a}$$

$$w^i = \frac{1}{RE^i} = 0, \quad \text{if } \phi^i > 2\sigma; i = POF, PCA, \text{ or } ASA \tag{1b}$$

where $w^i$ is the weighting factor for the corresponding phase-shift calculation method ($i = POF, PCA, \text{ and } ASA$). At each successive time point, the phase shift was estimated by halving the weighted average of the phase shifts calculated by the individual methods at the current time and adding the result to half of the previous moving-average value.

A moving standard deviation was calculated as the average standard deviation of the individual phase shifts found at all the previous time points. When the phase shift calculated by an individual method was an outlier ($\phi^i > 2\sigma$) compared to the other methods or to the historical values of the phase shift, the weighting factor $w^i$ for this term was set to 0. Namely, the contribution from this method was removed, and the phase shift for that sampling window was then calculated with the remaining methods. This weighting strategy minimizes the idiosyncratic responses of the individual methods, yielding a more robust estimation of the phase shift. When all three $\phi^i$ are outliers, the algorithm assumes that an abrupt change has occurred in the phase shift and restarts the running average. If such a rare event occurred in a future application, the radiation beam should be temporarily held. The detailed mathematical equations and evaluations were reported earlier.[32]

## Phase-Shift Correction for Improved External–Internal Correlation

The phase shift that was calculated for each sampling window was then corrected to dynamically boost the correlation between the external and internal waveforms. The enhanced correlation was compared with the original correlation. The MPD results were also validated against the TCC method, which maximizes the cross-correlation between the two signals. The time-domain and phase-domain methods are illustrated in Figure 1.

To correct the phase shift estimated by the TCC method, the navigator signal was shifted in time by an amount equal to the calculated phase shift divided by the waveform's frequency. The frequency of the waveform was estimated in four ways: the frequency at which the power spectrum of the bellows or navigator signals achieved their maximum value, and the average slope of the bellows' or navigator's instantaneous phase. At each time point, the frequency estimate was chosen to maximize the correlation between the waveforms following phase-shift correction. By comparing the correlation coefficient for the original waveforms to that of the phase-shift corrected waveforms, we assessed whether correcting the phase shift enhances the correlation between the external and internal signals.

## Applying Phase-Shift Correction in Respiratory-Gated Radiotherapy

To evaluate the usefulness of enhanced correlation after phase-shift correction, we examined a plausible clinical scenario wherein a 50% reduction in a tumor's motion margin is sought through RGRT. A theoretical threshold for triggering the radiation beam was set at the lower 30% of the bellows' amplitude (near the full exhalation) during the initial 10 s of each 4DMRI scan. In this hypothetical scenario, the radiation beam would turn on anytime the position of the bellows falls below the triggering threshold and the beam would turn off when the bellows rises above the threshold. This strategy aims to deliver radiation only when the navigator's position is within the lower 50% of its amplitude, and accordingly, a 50% motion margin should be applied in the RGRT planning. A somewhat conservative triggering threshold was selected to account for differences in the shapes of the external and internal waveforms. Because the phase shift does not account for baseline drift (although the standard 5.0 mm setup margin may account for some drift), periodic radiographic checking may be necessary to correct the potential baseline drift.

The gating accuracy was assessed by calculating the percentage of beam-on time (%harm) that radiation would have theoretically been delivered outside the motion margin before and after correcting the phase shifts estimated by the MPD and TCC methods. The median position of the navigator and 95%
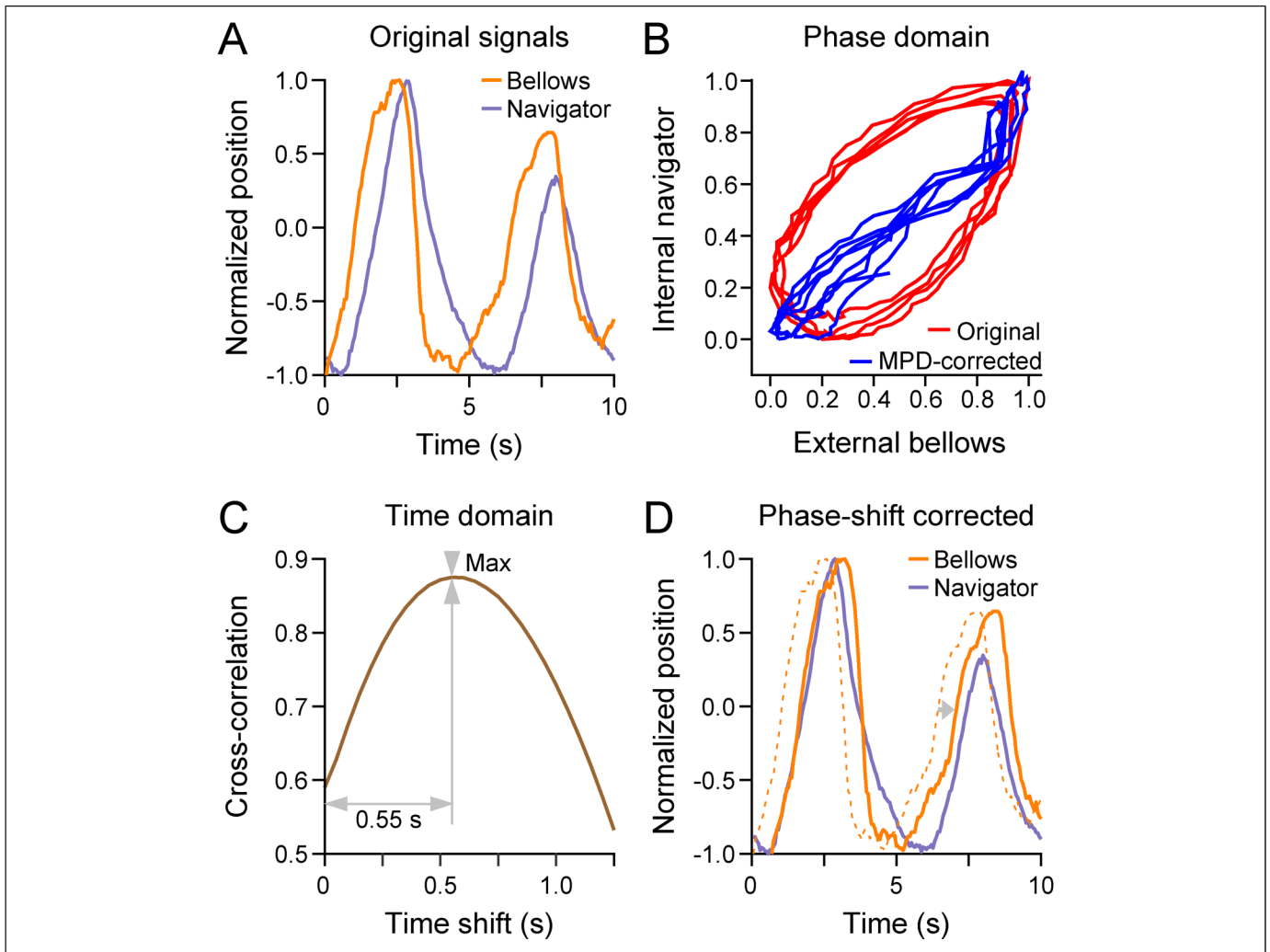
**Figure 1.** Methods for estimating the phase shift. (A) Example waveforms acquired by the external bellows (orange) and internal navigator (purple) for a healthy volunteer. The two waveforms reach their respective maximum values at different times, indicating the presence of a phase shift. (B) Ovoid trajectories (red) seen in a phase-space plot reiterate the existence of a phase shift between the external-bellows and internal-navigator waveforms. As was previously described, the phase shift can be efficiently estimated by a weighted average of three phase-domain techniques: best-fit oval, principal components analysis, and analytic signal analysis.[32] The trajectories in phase space become nearly linear (blue) after correction of the phase shift, reflecting an enhanced correlation between the external-bellows and internal-navigator waveforms. (C) The phase shift can also be estimated in the time domain by calculating the time shift that maximizes the cross-correlation between the two waveforms. (D) Correction of the phase shift—calculated by either method—translates the bellows waveform in time (gray arrow), thereby achieving a greater similarity and, consequently, a stronger correlation between the two waveforms.

confidence interval (CI) at the instant the radiation beam was triggered to turn on were also calculated before and after phase-shift correction.

## Results

### Dynamic Detection of Subject-Specific Phase Shifts in 2 Separate Scans

Table 1 tabulates the durations of the 2 4DMRI scans and the time sampling for phase-shift analysis in 10 volunteer subjects. Every scan lasted 5–16 min and a 15–20 m gap separated the pair of scans that each volunteer received. Because fewer image slices

are needed to span a volunteer's anterior-to-posterior dimension than that needed for the lateral direction, the coronal scans (scan 1) were shorter on average ($8.7 \pm 2.7$ m) than the sagittal scans (scan 2) ($11.8 \pm 2.2$ m). Across all of the scans, a total of 1213 time windows encompassing 114.9 m of data were analyzed.

Table 2 shows the estimated phase shifts for both scans using the MPD and TCC methods. The average phase shifts determined by the MPD method are approximately 1.00 radians (57° out of 360° or 16% of a breathing cycle) and are similar in both scans with a mean ratio of 1.07 ($p = .67$). The standard deviations are relatively small (<18%), except for two subjects in scan 1 (#4 and #10) and four volunteers in scan 2 (#5, #6, #7,

**Table 1.** Scan Time, Inter-Scan Gap, and Sampling Time for the Concurrently Acquired Motion Waveforms From 2 4dmri Scans Used in the Dynamic Phase-Shift Analyses of 10 Volunteers.

| Volunteer | Gender | Scan Length (m) | | Scan Gap (m) | No. of Time Windows[a] | | Time Analyzed (m) | |
|---|---|---|---|---|---|---|---|---|
| | | Scan 1 | Scan 2 | | Scan 1 | Scan 2 | Scan 1 | Scan 2 |
| 1 | ♀ | 6.5 | 12.1 | 20.4 | 6 | 50 | 0.8 | 4.6 |
| 2 | ♂ | 6.9 | 9.7 | 15.8 | 8 | 102 | 0.9 | 8.7 |
| 3 | ♂ | 9.4 | 9.6 | 16.9 | 16 | 44 | 2.0 | 4.3 |
| 4 | ♂ | 14.7 | 14.1 | 18.7 | 28 | 67 | 4.2 | 6.3 |
| 5 | ♀ | 8.8 | 16.1 | 29.7 | 68 | 153 | 6.3 | 14.2 |
| 6 | ♀ | 5.3 | 10.2 | 27.7 | 53 | 70 | 4.6 | 6.8 |
| 7 | ♂ | 8.2 | 9.6 | 16.5 | 63 | 83 | 5.5 | 7.8 |
| 8 | ♀ | 6.5 | 11.5 | 16.6 | 66 | 121 | 5.8 | 11.0 |
| 9 | ♂ | 9.7 | 11.6 | 18.6 | 12 | 103 | 1.6 | 9.3 |
| 10 | ♀ | 11.1 | 13.9 | 19.4 | 7 | 93 | 0.8 | 9.4 |
| Mean | | 8.7 | 11.8 | 20.0 | 32.7 | 88.6 | 3.3 | 8.2 |
| St Dev | | 2.7 | 2.2 | 4.8 | 26.7 | 33.2 | 2.2 | 3.0 |

[a]There are 1213 time windows in total and each contains 10 s.

and #9) who experienced higher breathing irregularities (23%–68%). The phase-shift ratio between scan 1 and scan 2 is $0.95 \pm 0.19$, excluding subjects 5 and 7 as 2 outliers. The TCC method calculates a smaller mean phase shift (0.85 radians), but usually yields a larger variation (ratio = 1.01, $p = .51$).

Figure 2 illustrates the phase-shift results based on both the MPD and TCC methods. For more than half of the volunteers, the phase shift was relatively stable throughout both scans using the MPD (Figure 2A) and TCC (Figure 2C) methods. The box-and-whisker diagrams reveal that the phase-shift distributions are usually broader for scan 2 (Figures 2B and 2D), an effect that may arise from having subjects participate in several breath-holding scans before the second 4DMRI scans. Notwithstanding differences in the distributions' spread, the median phase shifts in each pair of scans are similar, except for subjects 7 and 9. Some scattered outliers in the phase-shift distributions were caused by extreme breathing irregularities.

## Enhanced Motion Correlation with Dynamic Phase-Shift Correction

Plotting the phase shifts and the initial correlations on the same time axis reveals that the two variables nearly mirror each other, suggesting an inverse relationship: low initial correlations are associated with large phase shifts (Figures 3A and 3B). For most of the volunteers, correcting the phase shift yields a correlation curve close to 1.0 in almost every time window. Examining the relationship between the phase shift and the initial correlation for the 1213 sampling windows analyzed for all 10 volunteers provides further evidence of the inverse relationship (Figures 3C and 3D). Indeed, the Pearson's correlation coefficient between the MPD phase shifts and initial correlations is −0.93, and a zero-parameter fit to the line, Initial Correlation = $1 - (2/\pi)*abs(\phi^{MPD})$, yields an average residual error of 0.16. Better agreement is found for the curve, Initial Correlation = $\cos(\phi^{MPD})$, which yields an average residual error of 0.07 (Figure 3C, top). Correcting the MPD phase

shift enhances the correlation between the navigator and bellows waveforms in 92.25% ( = 1109/1213) of the analyzed sampling windows. On average, the correlation rose by 0.37 after correcting the phase shift (Figure 3C, bottom).

In the 94 sampling windows (or 7.75%) for which phase-shift correction worsened the correlation, the correlation decrease exceeded 0.1 in only 20 windows (21.3%). Interestingly, 76 of the 94 windows (80.9%) with worse correlation belong to volunteer 5, who had the smallest average phase shift and, consequently, one of the highest uncorrected correlations (0.80 in scan 1 and 0.83 in scan 2), leaving little room for further improvement. Additionally, the shapes of this volunteer's waveforms are much broader in the bellows than in the navigator, making the optimal phase shift ambiguous and leading to a slightly worse correlation between the two waveforms at some time points using the MPD method. In all sampling windows for subject 5, however, the overall mean correlation is still enhanced to a correlation of 0.86 in scan 1 and unchanged in scan 2.

Pearson's correlation coefficient between the TCC phase shifts and initial correlations is −0.89, and a zero-parameter fit to the line, Initial Correlation = $1 - (2/\pi)*abs(\phi^{TCC})$, yields an average residual error of 0.12, and the average residual error was 0.15 for the curve, Initial Correlation = $\cos(\phi^{TCC})$ (Figure 3D, top). Because the TCC method maximizes the cross-correlation between the bellows and navigator waveforms, correcting the TCC phase shift never worsened the correlation. Across all sampling windows, the correlation rose by 0.40 on average and was uncharged in only 10 windows (0.82%) (Figure 3D, bottom).

Table 3 provides the quantitative correlation enhancements for both scans using the MPD and TCC methods. Averaged across all 10 volunteers, the correlation increases substantially from $0.56 \pm 0.22$ for the original navigator and bellows waveforms to $0.85 \pm 0.11$ ($p = .0003$) after correcting the MPD phase shift and to $0.89 \pm 0.06$ ($p = .0002$) after correcting the TCC phase shift in scan 1, and from $0.47 \pm 0.30$ to $0.84 \pm 0.08$

**Table 2.** Phase shifts (in radians) determined by Both the Mean Phase-Domain (MPD) Method and the Time-domain Cross-correlation (TCC) method in 4DMRI scan 1 and scan 2.

| | Phase Shifts (Radian) by MPD method | | | | | Phase Shifts (Radian) by TCC method | | | | |
| | Scan 1 | | Scan 2 | | | Scan 1 | | Scan 2 | | |
| Subject | Mean | SD | Mean | SD | Ratio of 2 means | Mean | SD | Mean | SD | Ratio of 2 means |
|---|---|---|---|---|---|---|---|---|---|---|
| 1 | 0.67 | 0.01 | 0.74 | 0.05 | 0.91 | 0.58 | 0.04 | 0.63 | 0.10 | 0.92 |
| 2 | 1.00 | 0.02 | 1.22 | 0.08 | 0.82 | 0.84 | 0.04 | 0.98 | 0.20 | 0.86 |
| 3 | 0.59 | 0.04 | 0.55 | 0.03 | 1.07 | 0.55 | 0.06 | 0.51 | 0.05 | 1.08 |
| 4 | 1.17 | 0.32 | 1.27 | 0.18 | 0.92 | 1.16 | 0.35 | 1.23 | 0.42 | 0.94 |
| 5 | 0.65 | 0.10 | 0.28 | 0.48 | 2.32 | 0.43 | 0.09 | 0.21 | 0.31 | 2.05 |
| 6 | 0.99 | 0.16 | 1.02 | 0.23 | 0.97 | 0.79 | 0.22 | 0.84 | 0.47 | 0.94 |
| 7 | 0.97 | 0.07 | 1.60 | 0.24 | 0.61 | 0.86 | 0.15 | 1.57 | 0.27 | 0.55 |
| 8 | 1.57 | 0.03 | 1.55 | 0.08 | 1.01 | 1.33 | 0.26 | 1.34 | 0.29 | 0.99 |
| 9 | 0.96 | 0.14 | 1.24 | 0.35 | 0.77 | 0.85 | 0.22 | 1.14 | 0.38 | 0.75 |
| 10 | 1.07 | 0.73 | 0.84 | 0.13 | 1.27 | 0.57 | 0.37 | 0.59 | 0.20 | 0.97 |
| Mean | 0.96 | 0.16 | 1.03 | 0.19 | 1.07 | 0.80 | 0.18 | 0.90 | 0.27 | 1.01 |
| SD | 0.29 | 0.22 | 0.41 | 0.14 | 0.45 | 0.28 | 0.12 | 0.40 | 0.13 | 0.38 |
| *p*-value | 0.67 | | | | | 0.51 | | | | |

($p = .002$) after MPD correction and to $0.87 \pm 0.06$ ($p = .001$) after TCC correction in scan 2. Both methods yield similar enhancements in the correlation between the bellows and navigator waveforms. The set of mean enhanced correlations for the 10 volunteers after correcting the MPD phase shift is indistinguishable from that for the TCC method ($p = .33$ for scan 1, $p = .31$ for scan 2), and the %Diff between the two methods averaged across all 10 volunteers is $0.06 \pm 0.11$ in scan 1 and $0.04 \pm 0.03$ in scan 2.

A statistically significant enhancement in the correlation was found for every volunteer in both scans after correcting the TCC phase shift and for all, except for volunteer 5 in scan 2 and for volunteer 10 in scan 1, after correcting the MPD phase shift (Figure 4). For volunteer 5 in scan 2, despite yielding a worse correlation in 72 of 153 windows (47.1%), correction of the MPD phase shift produced an average correlation that was no different than the average uncorrected correlation. For volunteer 10 in scan 1, only 7 sampling windows were available for analysis likely contributed to the correlation enhancement not reaching statistical significance after correcting the MPD phase shift.

## Improvement in Respiratory-Gated Radiotherapy via Correlation Enhancement

Figure 5 illustrates how correcting the phase shift improves the accuracy of amplitude-triggered respiratory gating around full exhalation. By translating the bellows signal in time, phase-shift correction shifts the beam-on window to within the navigator's acceptable motion margin: the bellows triggers the radiation beam to turn on at more appropriate times and the %harm (percentage of beam-on time that radiation is delivered outside the motion margin) to the patient is reduced. Table 4 tabulates each volunteer's motion margin, the median, and 95% CI for the navigator's position at the instant the beam turns on, and the %

harm. Before correcting the phase shift, only 4 cases achieve acceptable gating, defined as <10% harm. The number of cases achieving acceptable gating increases to 9 cases after correcting the MPD phase shift and to 17 cases after the TCC correction. Baseline drifts—with respect to the navigator's position during the initial 10 s of a scan—occur in some cases and result in negative values for the lower bound of the 95% CI. The baseline drifts cannot be rectified by phase-shift correction, but maybe addressed by including a 5.0 mm setup margin.

## Discussion

### Subject-Specific Phase Shifts Estimated by the Phase- and Time-Domain Methods

By combining three individual methods with each weighted by the reciprocal of its estimated RE (see Eq. 1), the MPD method succeeds in detecting the phase shift and enhancing the internal–external correlation in more than 99% of the analyzed time windows. The 10 s windows were advanced in time by 5 s increments—dynamically updating the window by adding 5 s of new data and removing 5 s of old data—to capture approximately one new breathing cycle in each window. The moving time window allows dynamic phase-shift detection, produces a robust phase-shift estimation, and minimizes the impact of sudden breathing irregularities. This may suggest the origin of the stability of the subject-specific phase shifts, even with large breathing irregularities, as shown in Figures 2 and 3.

The results of phase-shift detection and motion correlation enhancement are confirmed by the TCC method. If a low correlation arises from a phase shift between two waveforms, then the phase shift should be observed in both the phase and time domains. The close agreement in the correlation enhancement achieved by the phase-domain and time-domain methods
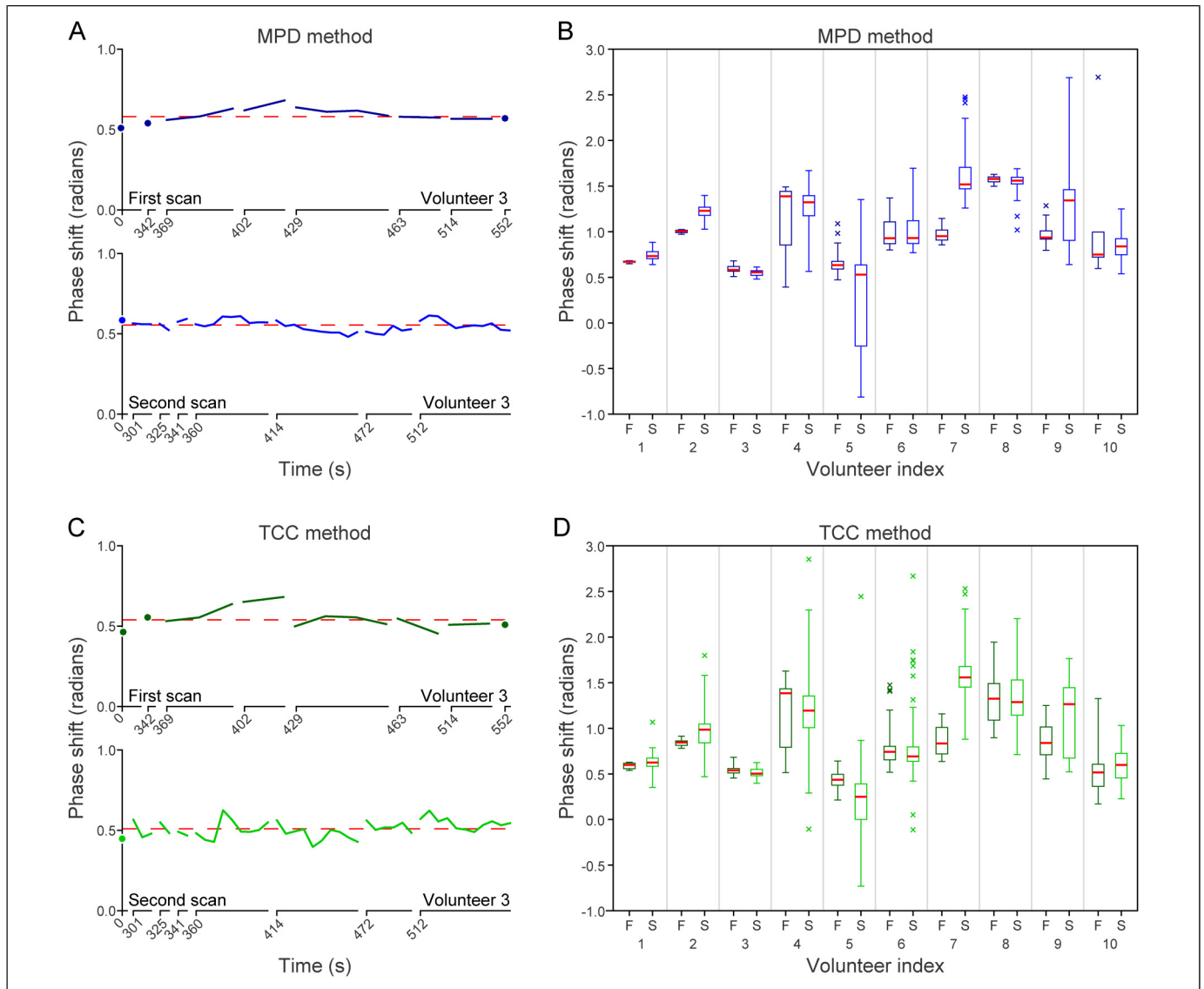
**Figure 2.** Phase-shift distributions across two scans. (A) Phase shifts were calculated by the mean phase-domain (MPD) method for the first (top) and second (bottom) scans of volunteer 3. Each listed time indicates the beginning of a time segment, and each point on the curve marks the phase shift for a 10-s window. The dashed, red line indicates the median phase shift for each scan. (B) Box-and-whisker diagrams portray the distributions of the phase shifts estimated by the MPD method during the first (F) and second (S) 4D-MRI scans for each of the 10 volunteers. The red, horizontal lines indicate the median of each distribution, the boxes encompass the middle two quartiles, the whiskers span each distribution's range, and the xs mark outliers that are three or more interquartile lengths below the lower quartile or above the upper quartile. The distributions appear similar for half of the volunteers (1, 3, 6, 8, and 10). (C, D) The phase-shift results for the time-domain cross-correlation (TCC) method are portrayed as for panels A and B.

suggests an accurate estimation of the phase shift and accords with the proposition that the phase shift constitutes the primary cause of the originally weak correlations between the bellows and navigator waveforms. The consistency of the results from two independent approaches indicates that phase-shift correction is an effective means to enhance the external–internal correlation.

Based on clinical observations of patients' breathing behaviors,[16,29,35,36] it was reasonable to hypothesize that some patient-specific respiratory features, including the phase shift, may remain relatively invariant over a short period, such as 30 min. Physiologically, thoracoabdominal movements during respiration are initiated by a joint effort of the diaphragm and intercostal muscles, which can be quantified as the ratio of thoracic to abdominal involvement during respiration.[21] Because little volitional control is exerted over respirations during free-breathing, human subjects exhibit their natural breathing behavior—governed by involuntary muscle actions—in this state. A phase shift should therefore represent a fundamental feature of an individual's free-breathing pattern, and differences in anatomy and physiology will engender variation among subjects in the magnitudes of their respiratory phase shifts.
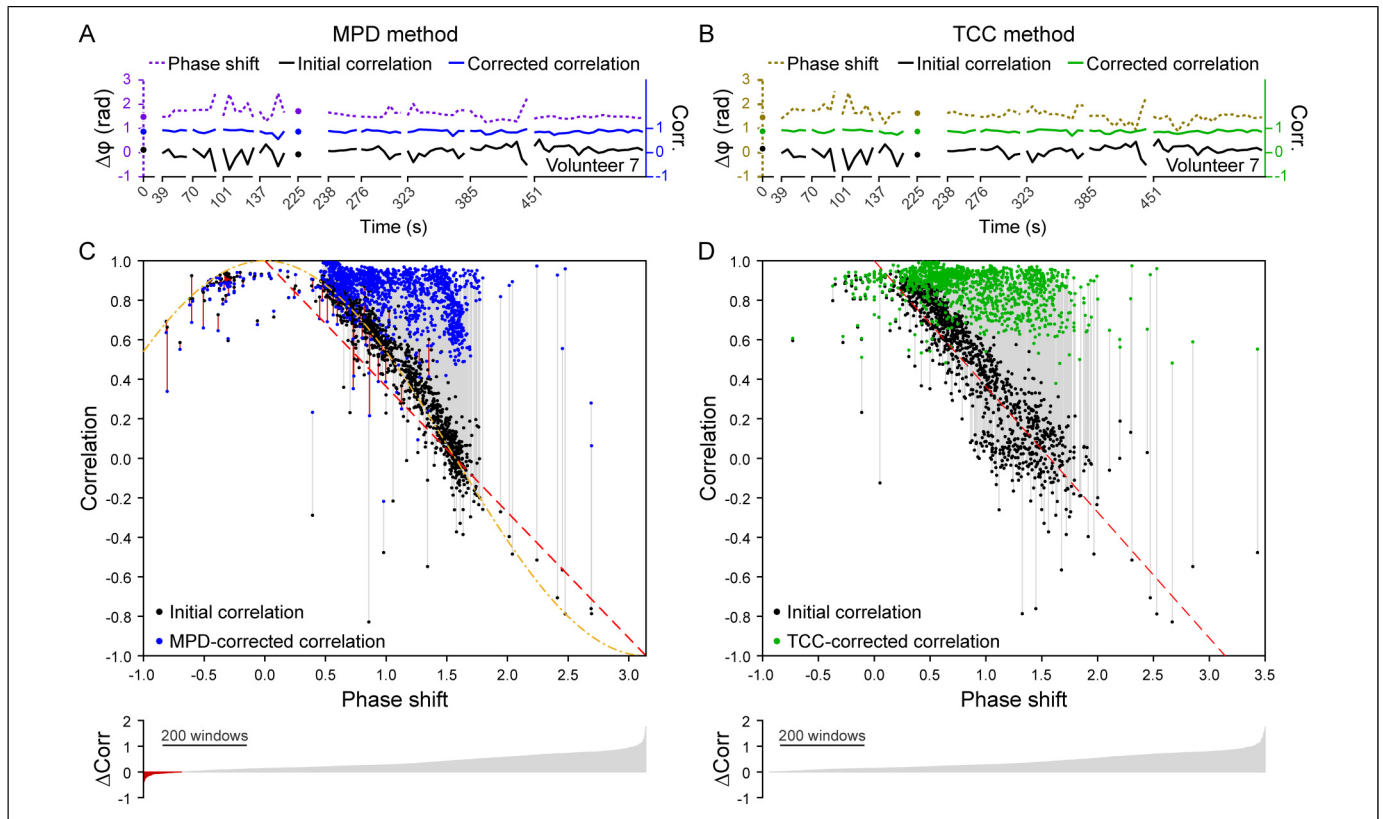
**Figure 3.** An inverse relationship exists between the phase shift and initial correlation. (A) Phase shifts estimated by the MPD method (dashed, purple curves), the initial correlation between the bellows and navigator waveforms (solid, black curves), and the correlation between the waveforms after phase-shift correction (solid, blue curves) (mean = 0.87 ± 0.07) for volunteer 7. (B) Phase shifts estimated by the TCC method (dashed, gold), the initial correlation between the bellows and navigator waveforms (solid, black), and the correlation between the waveforms after phase-shift correction (solid, green). (C) Each black point in the scatter plot (top panel) indicates the calculated MPD phase shift and initial correlation between the bellows and navigator waveforms for a single time window. This relation is reasonably described by Initial Correlation = $1 - 2*abs(\phi)/\pi$ (red, dashed line) and even better described by Initial Correlation = $\cos(\phi)$ (orange, dashed curve). Each black point is paired with a blue point that indicates the correlation between the waveforms following phase-shift correction; vertical gray lines indicate improved correlations and vertical red lines indicate correlations that were worse. Sorting the change in correlation from least to greatest for the 1213 time-segment windows from all 10 volunteers (bottom panel) illustrates that enhancement of the correlation was achieved for 1119 windows (92.25%). (D) The TCC results are shown in the same fashion, but no correction reductions (red lines) are observed, resulting in 100% improvement.

Although many individuals may exhibit irregularities in the amplitude and frequency of their breathing patterns, switching between classes of breathing patterns—such as from chest breathing to belly breathing—usually requires voluntary actions. Whereas inhalation is an active process triggered by contraction of the diaphragm and intercostal muscles, exhalation is a passive process of muscle relaxation and is consequently more reproducible, particularly the state of a full exhalation. The relationship between external surface motion and internal muscle action should, consequently, remain steady with mild fluctuations.[32] The detected phase shift does, in fact, fluctuate (Figures 3A and 3B and Table 2), but the enhanced correlation, nevertheless, is fairly stable over time (Figures 3C and 3B and Table 3) owing to its tolerance to small, residual phase shifts estimated by either the MPD or TCC method (further discussion is provided in the following sub-section).

Numerous physiological and technical factors contribute to the phase shifts that are detected between the motions of internal and external structures. Unlike the real-time position management (RPM) that senses the motion of the body's anterior surface, the bellows senses the pressure differences around the circumference (or perimeter) of the body during respiration. In fact, a phase shift between the RPM and bellows was previously reported.[37] When it is placed just inferior to the xiphoid process of the sternum, the bellows encircles the lateral and posterior ribs and therefore senses the movements of both the diaphragm and the intercostal muscles. By contrast, the internal navigator senses only the motion of the diaphragm. The external and internal surrogates therefore represent somewhat different motions. These differences arise, in part, from the motion delays engendered by the elasticity of the soft tissues that separate the internal and external structures. If the bellows is instead placed around the umbilicus, the rib cage and the

**Table 3.** Correlation Enhancement Following Phase-Shift Corrections in Both Scans Using the MPD Method or the TCC Method[a].

| Subject | Correlation enhancement in Scan 1 | | | | | | | Correlation enhancement in Scan 2 | | | | | | |
| --- | --- | --- | --- | --- | --- | --- | --- | --- | --- | --- | --- | --- | --- | --- |
| | Original | | By MPD | | By TCC | | %Diff[b] | Original | | By MPD | | By TCC | | %Diff* |
| | Mean | SD | Mean | SD | Mean | SD | | Mean | SD | Mean | SD | Mean | SD | |
| 1 | 0.79 | 0.01 | 0.96 | 0.01 | 0.96 | 0.01 | 0.00 | 0.72 | 0.10 | 0.90 | 0.05 | 0.91 | 0.05 | 0.01 |
| 2 | 0.59 | 0.04 | 0.93 | 0.01 | 0.94 | 0.01 | 0.01 | 0.40 | 0.11 | 0.79 | 0.12 | 0.83 | 0.10 | 0.05 |
| 3 | 0.81 | 0.05 | 0.96 | 0.03 | 0.96 | 0.03 | 0.00 | 0.85 | 0.03 | 0.98 | 0.01 | 0.99 | 0.01 | 0.01 |
| 4 | 0.33 | 0.25 | 0.86 | 0.15 | 0.87 | 0.12 | 0.01 | 0.28 | 0.25 | 0.85 | 0.15 | 0.88 | 0.09 | 0.04 |
| 5 | 0.80 | 0.09 | 0.88 | 0.09 | 0.91 | 0.07 | 0.03 | 0.83 | 0.11 | 0.83 | 0.13 | 0.88 | 0.08 | 0.06 |
| 6 | 0.59 | 0.14 | 0.87 | 0.09 | 0.90 | 0.07 | 0.03 | 0.52 | 0.27 | 0.82 | 0.14 | 0.86 | 0.12 | 0.05 |
| 7 | 0.58 | 0.10 | 0.91 | 0.04 | 0.92 | 0.04 | 0.01 | 0.05 | 0.23 | 0.87 | 0.07 | 0.88 | 0.06 | 0.01 |
| 8 | 0.10 | 0.09 | 0.70 | 0.09 | 0.76 | 0.06 | 0.09 | 0.03 | 0.10 | 0.69 | 0.10 | 0.75 | 0.08 | 0.09 |
| 9 | 0.53 | 0.15 | 0.82 | 0.09 | 0.83 | 0.09 | 0.01 | 0.36 | 0.30 | 0.87 | 0.10 | 0.88 | 0.08 | 0.01 |
| 10 | 0.47 | 0.56 | 0.64 | 0.31 | 0.87 | 0.09 | 0.36 | 0.66 | 0.13 | 0.82 | 0.11 | 0.88 | 0.08 | 0.07 |
| Mean | 0.56 | 0.15 | 0.85 | 0.09 | 0.89 | 0.06 | 0.06 | 0.47 | 0.16 | 0.84 | 0.10 | 0.87 | 0.08 | 0.04 |
| SD | 0.22 | 0.16 | 0.11 | 0.09 | 0.06 | 0.04 | 0.11[c] | 0.30 | 0.09 | 0.08 | 0.04 | 0.06 | 0.03 | 0.03 |
| p-value | .0003 | | | | .0002 | | | .0012 | | | | .0005 | | |

[a]Both methods provide similar correlation enhancement. Overall, the correlation enhancements are all significant, except for subject 10 in scan 1 and subject 5 in scan 2 using the MPD method.

[b]%Diff = $(r_2 - r_1)/r_2 \times 100\%$ is between MPD-corrected and TCC-corrected correlations.

[c]This SD is distorted by the outlier from patient 10 and does not accurately represent the actual distribution.

9
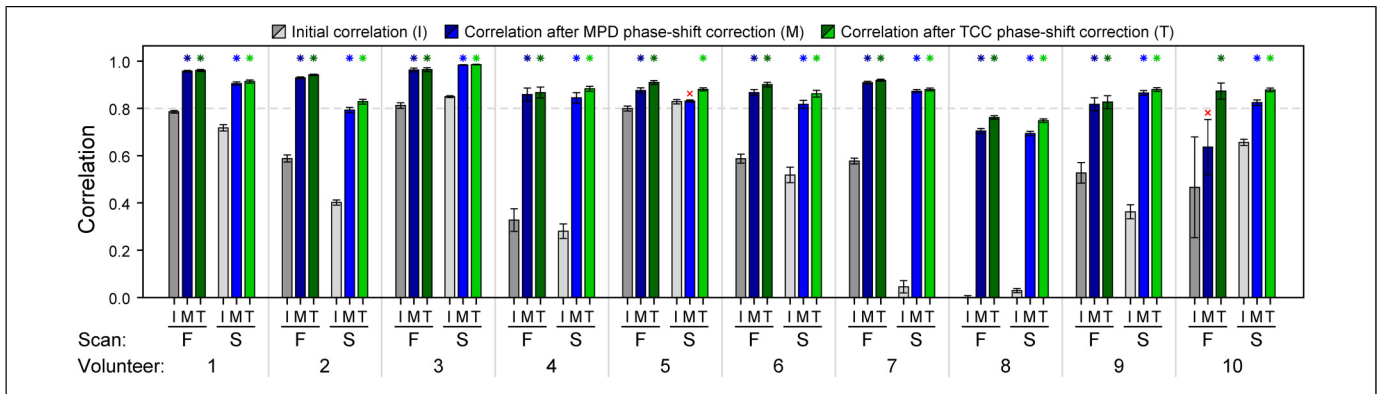
**Figure 4.** Phase-shift correction enhances the correlation between bellows and navigator waveforms. A bar chart portrays the mean correlation and standard error before (I, gray bars) and after correcting the MPD (M, blue bars) or TCC (T, green bars) phase shift for every volunteer in both the first scan (F, darker shades) and second scan (S, lighter shades). An asterisk indicates that the underlying bar represents a statistically significant enhancement compared to the initial correlation, $p < .05$. Correcting the TCC phase shift succeeded in enhancing the correlation in both scans for every volunteer. A statistically significant correlation enhancement was not achieved by correcting the MPD phase shift throughout the second scan for volunteer 5 or the first scan for volunteer 10 (red "x"). The dashed, gray line marks a correlation of 0.8 for reference.
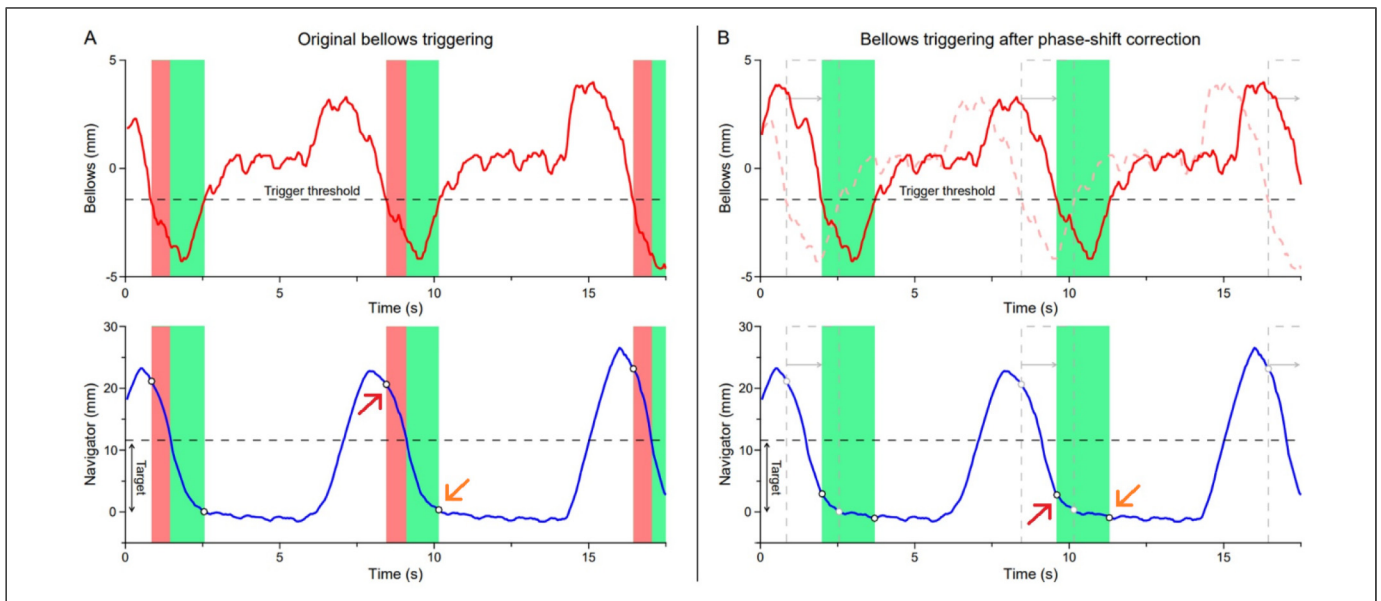


**Figure 5.** Phase-shift correction improves the accuracy of amplitude-triggered respiratory gating. A theoretical threshold for triggering the radiation beam to turn on is set at 30% of the bellows' amplitude from the initial 10s of a 4DMRI scan (dashed, horizontal line in the top graphs) and an acceptable margin for internal motion is set at 50% of the navigator's amplitude during the same timeframe (dashed, horizontal line in the bottom graphs). Based on the gating strategy, the colored areas indicate the times that the radiation beam would theoretically be on. (A) Before correcting the phase shift, the beam-on is triggered before the navigator reaches the acceptable motion margin and causes theoretical harm; the red areas encompass the times that the beam is aberrantly turned on. The %harm is calculated as the sum of the widths of the red areas divided by that of the red and green areas. The red arrows indicate the navigator's position at the instant beam-on time; the median and 95% CI for these positions are tabulated in Table 4. (B) After correcting the phase shift, the bellows triggers the beam-on entirely within the navigator's motion margin, yielding 100% gating accuracy in this example (green areas). Because the bellows most often leads the navigator, the radiation beam usually turns off (orange arrows) well within the navigator's motion margin and does not contribute to the theoretical harm. Because the shapes of the bellows and navigator waveforms differ significantly, the bellows-triggered gating is inefficient and remains an area of active investigation.

motion of the intercostal muscles contained therein are excluded. In this scenario, the bellows may primarily sense the motion caused by the diaphragm and a phase shift that differs from that for placing the bellows at the xiphoid may be obtained.[4,38] In summary, surrogate types and placements, muscle-engagement profiles, tissue elasticities, and variations in breathing patterns may all affect measured phase shifts.[4,35,39,40] Notwithstanding the complexity of the

**Table 4.** The Motion Margin, the Median, and 95% Confidence Interval (CI) for the Navigator's Position at the Instant the Beam Turns On, and the Percentage of Harm (Percentage of Beam-On Time That Radiation Is Delivered Outside The Motion Margin) Before and After Correcting the MPD and TCC Phase Shifts[a].

| Imaging session | Vol | Motion margin (mm) | Original | | | After MPD correction | | | After TCC correction | | |
|---|---|---|---|---|---|---|---|---|---|---|---|
| | | | median (mm) | 95% CI (mm) | % harm | median (mm) | 95% CI (mm) | % harm | median (mm) | 95% CI (mm) | % harm |
| Scan 1 | 1 | 5.0 | 6.6 | 4.8–6.9 | 15 | 5.9 | 4.5–6.5 | 9 | 4.7 | 2.7–4.9 | 0 |
| | 2 | 6.8 | 8.2 | 0.7–11.0 | 16 | 6.2 | 0.5–8.9 | 4 | 3.1 | 0.5–4.5 | 0 |
| | 3 | 7.7 | 19.2 | 8.9–43.7 | 41 | 16.6 | 6.7–37.6 | 39 | 13.7 | 3.8–28.5 | 37 |
| | 4 | 2.8 | 0.8 | −1.1–4.2 | 6 | 0.6 | −1.0–3.7 | 4 | 0.4 | −1.3–2.9 | 1 |
| | 5 | 8.8 | 19.3 | 9.6–41.2 | 60 | 17.7 | 8.3–39.4 | 59 | 16.6 | 7.1–36.5 | 58 |
| | 6 | 7.7 | 10.4 | −4.0–38.5 | 19 | 7.4 | −3.3–30.5 | 11 | 3.6 | −3.7–14.7 | 5 |
| | 7 | 7.7 | 5.7 | 0.3–27.0 | 33 | 4.2 | 0.0–23.9 | 25 | 2.7 | 0.1–15.3 | 16 |
| | 8 | 11.6 | 20.8 | 1.1–30.3 | 45 | 15.1 | 0.5–24.9 | 18 | 3.1 | 0.0–10.6 | 0 |
| | 9 | 3.6 | 0.2 | −1.1–6.1 | 8 | 0.2 | −1.1–5.2 | 3 | 0.2 | −0.9–3.2 | 0 |
| | 10 | 12.0 | 6.2 | 0.0–19.3 | 5 | 4.5 | −0.2–14.5 | 2 | 3.1 | −0.2–10.6 | 0 |
| | Avg | | | | 25 | | | 17 | | | 12 |
| | SD | | | | 19 | | | 19 | | | 20 |
| Scan 2 | 1 | 6.9 | 7.0 | 0.3–11.6 | 13 | 6.1 | 0.1–10.5 | 7 | 4.8 | 0.4–8.2 | 1 |
| | 2 | 6.9 | 10.2 | 2.2–18.6 | 32 | 6.4 | 1.5–12.9 | 11 | 2.2 | 0.6–5.7 | 0 |
| | 3 | 9.1 | 11.3 | 6.4–21.7 | 10 | 9.6 | 5.4–18.4 | 5 | 6.6 | 3.0–12.2 | 1 |
| | 4 | 35.0 | 65.9 | 1.7–117.6 | 40 | 57.9 | 0.2–39.6 | 25 | 19.9 | 1.0–40.2 | 1 |
| | 5 | 11.0 | −1.3 | −9.7–18.0 | 3 | −1.9 | −9.7–18.7 | 3 | −2.3 | −9.8–17.4 | 3 |
| | 6 | 7.7 | 7.1 | 1.4–23.7 | 23 | 4.8 | 0.7–16.2 | 9 | 2.7 | −0.4–5.5 | 6 |
| | 7 | 9.1 | 19.3 | 1.5–34.0 | 58 | 16.8 | 0.2–26.0 | 40 | 7.5 | 0.2–18.5 | 7 |
| | 8 | 6.6 | 16.1 | 1.7–24.3 | 53 | 10.8 | 1.4–19.5 | 21 | 2.5 | 0.7–5.5 | 0 |
| | 9 | 4.0 | 1.4 | −0.6–15.7 | 35 | 1.3 | −0.6–11.1 | 22 | 1.0 | −0.6–6.5 | 3 |
| | 10 | 14.0 | 5.2 | −7.6–53.2 | 17 | 3.6 | −7.6–39.1 | 10 | 2.8 | −7.8–29.7 | 5 |
| | Avg | | | | 28 | | | 15 | | | 3 |
| | SD | | | | 18 | | | 11 | | | 3 |

[a]Among 20 cases of 10 volunteers (vol), only 4 cases produce <10%harm before phase-shift correction, but the number increases to 9 cases after the MPD correction and to 17 cases after the TCC correction. A negative value in the lower bound of the 95% CI indicates a baseline drift in the navigator from its position during the initial 10 s of the 4DMRI scan. Because the baseline drift is independent of the phase shift, neither method for correcting the phase shift can rectify the drift. Five cases contain drifts that exceed 5.0 mm and cannot be addressed by a 5.0 mm setup margin.

phenomenon, the phase shift may be stable during involuntary free-breathing, possibly until a voluntary action occurs.

## The Stability and Reproducibility of the Subject-Specific Phase Shift and Correlation Enhancement

In this study, the average ratio of the phase shifts estimated by the MPD between the two scans is $1.07 \pm 0.45$ ($0.95 \pm 0.19$, excluding 2 outliers: patients 5 and 7), illustrating a rather reproducible phase shift over 30 min. On average, the correlation is enhanced from $0.56 \pm 0.22$ to $0.85 \pm 0.11$ in scan 1 and from $0.47 \pm 0.30$ to $0.84 \pm 0.08$ in scan 2 by correcting the phase shifts detected by the MPD method. For the two subjects with the largest phase shifts (1.2 and 1.6 radians for subjects 4 and 8, respectively) and no apparent initial correlation ($r = 0.33$ and $r = 0.10$), correcting the phase shift enhances the correlation to 0.86 and 0.70 in scan 1 and to 0.85 and 0.69 in scan 2, respectively. Correcting the phase shift reliably enhances the correlation to above 0.8 over timeframes lasting up to—and perhaps exceeding—30 min in 8 out of 10 subjects for the MPD method and in 9 out of 10 subjects for the TCC method. Phase-shift correction, therefore,

exhibits the fidelity and stability that are requisite criteria for clinical applications.

There is close agreement (%Diff $\leq 0.05$) between the correlation enhancements attained by the MPD and TCC methods for 8 subjects in scan 1 and for 7 subjects in scan 2. Although the performances of the MPD and TCC methods are comparable, focusing on the phase shift, rather than on the more variable time shift, may allow algorithms that correct the shift between respiratory waveforms to update less frequently while still achieving a steady, enhanced correlation.

In accord with previously reported findings for external–internal motion models, the degree of correlation enhancement achieved in this study indicates that the phase shift is the primary cause for the initially low correlations.[41,42] Aside from the phase shift, baseline drifts in the respiratory waveforms may also degrade the correlation between external and internal motions.[31] A baseline drift would certainly affect the targeting during radiotherapy and should consequently be corrected in correlation-based models for predicting tumor motion. Because a baseline drift unfolds over low frequencies, it could be represented as a separate, dedicated term in a prediction model, rather than entangling this process with the

respiratory correlation term. In a simplified model, a baseline drift could even be regarded as linear over the timeframe of a few breathing cycles, but exploring this phenomenon is beyond the scope of the current investigation.

## Correlation Enhancement by Dynamic Phase-Shift Correction Using the MPD Method

The temporal resolution of the phase-shift calculation by the MPD method is approximately equal to the length of the time window, which should cover at least one breathing cycle. Time windows encompassing 12.5 s and 7.5 s of data were previously examined and produced results that were similar and statistically indistinguishable from the results obtained with the10 s windows, suggesting that any of these window lengths are reasonable choices. Owing to its limited temporal resolution, the MPD method tracks slow changes in the phase shift well but may lag behind abrupt changes by the length of a time window. In this study, a small number of sharp changes are observed in the TCC-estimated phase shift, suggesting that rapid changes in the phase shift occur only occasionally and that the 10 s resolution of the MPD method is adequate to track changes in rather stable phase shifts. As discussed above, even if the phase-shift detection fails to adapt rapidly to a fast-changing event, the impact on the correlation enhancement should be minimal owing to a moderate tolerance for uncertainties in the phase shift. The fact that the phase shift remains relatively steady over 30 min for most subjects suggests a simple solution to improve respiratory-motion management during gated radiotherapy. For clinical applications, however, a combination of the TCC and MPD methods may be applied to balance the shortcomings of each method and enable even more robust predictions.

In this study, the MPD method fails to produce a phase-shift estimate in only ~0.1% of the analyzed time windows, meaning that all three individual methods failed simultaneously. Abrupt breathing irregularities may occur in these rare events, producing—for example—a phase-domain trajectory that resembles two disparately oriented ovals that, together, cannot be accurately represented by a single ellipse, and throws off the MPD calculation. After subdividing such a time window into two parts that each contained only one of these ovals, the MPD method succeeded in estimating phase shifts of approximately 1.45 radians, values that are similar to phase shifts found for subsequent time windows. The sudden reorientation of the phase-space trajectory may reflect an abrupt change in the subject's breathing pattern. When these rare events are detected, the treatment beam can be temporarily held, like gating, until the MPD method is again able to estimate the phase shift.

## The Potential Usefulness of Phase-Shift Correction in Respiratory-Gated Radiotherapy

Correcting the phase shift improves the validity of the amplitude-triggered gating technique (see Figure 5). To account for the large uncertainties—even after phase-shift

correction—in predicting the motion of an internal organ, we chose a conservative threshold for triggering the radiation beam. Setting the triggering threshold at 30% of the bellows' amplitude from full exhalation ensures that the majority of radiation would be delivered within an acceptable motion margin, defined to be 50% of the navigator's amplitude. Before correcting the phase shift, only 4 out of 20 cases achieve acceptable gating, defined as <10%harm. After correcting the phase shift, the number of cases that achieve acceptable gating rises to 9 cases using the MPD correction and to 17 cases using the TCC correction. The significant improvement in the number of cases that are suitable for RGRT suggests a potential clinical role for phase-shift correction.

Baseline drifts in the navigator waveforms were observed in some of the scans. The lower bound in the 95% CI of the navigator's position when the radiation beam is turned on should ideally be close to zero: an upward baseline shift would tend to increase the value of this lower bound and a downward shift would tend to decrease the value. The drift cannot be rectified by correcting the phase shift, but the 5.0 mm setup margin can cover most minor baseline drifts. There are, however, 5 cases (25%) wherein the baseline drift exceeds 5.0 mm. Monitoring the baseline over a longer scan period—which should better represent the averaged respiratory baseline—may help identify a more appropriate setup margin for the individual patient. For a long-term baseline drift at treatment, it may become necessary to shift the couch to reset the baseline to zero or even redo the setup.

We examined how phase-shift correction affects amplitude-triggered respiratory gating. Phase gating is also employed as an alternative strategy to account for respiratory motion. Regardless of the gating scheme, the gating window is usually determined at simulation by a physician based on 4DCT, such as 30–70% as the gating window (50% is the full exhalation). For amplitude-gated treatment, it can be converted to an amplitude-gating window.[43] In general, phase gating depends on online phase determination and is more sensitive to breathing irregularities.[43,44] The MPD method can offer online phase determination with high accuracy and resolution (compared with the 10-bin 4DCT at simulation), showing the potential to improve the robustness of phase gating. Additionally, a stable phase shift between external and internal motions can also help the phase gating to treat an internal target. Therefore, by evaluating the variability of a patient's phase shift during simulation, the MPD method could identify suitable candidates with stable phase shifts for phase-gated radiotherapy.

## Clinical Considerations for Potential Phase-Shift-Corrected External Surrogates

Because this study focuses on healthy volunteers, the movement of the diaphragm—the organ with the greatest superior-to-inferior motion during free-breathing—was monitored. In patients, the same methodology used for tracking the diaphragm's motion can be applied instead of monitoring the motion of lung or liver tumors. Specifically, it is possible to

place a small navigator window on the tumor–lung interface to measure the motion of a sizable lung tumor, i.e., a tumor whose diameter exceeds 2 cm. Alternatively, the time-resolved 4DMRI with a 2 Hz frame rate[36,45–47] can be applied to investigate the correlation between the motions of an external structure and an internal tumor. Depending on the clinical needs, the dynamic MR imaging data can be used to build either a simple phase-shift-corrected respiratory model or a sophisticated physics-based perturbation model using surface-imaging-based spirometry as a surrogate.[48,49]

Diaphragm motion, which has been investigated as an important surrogate for predicting the motion of lung and liver cancers,[50–52] is readily detected using fluoroscopic imaging in the clinic.[53] A study has illustrated only a slight superiority of correlating an external motion with multiple internal surrogates compared to a single internal surrogate.[54] Therefore, a method that enhances the correlation between the bellows and diaphragm motions could be extended to predict tumor motion with only minor modifications.

Based on the results from this study, patients could be categorized in terms of their external–internal motion correlation into three groups: (1) naturally high correlation, (2) enhanced high correlation, and (3) enhanced correlation but not high enough. This study has demonstrated that phase-shift correction can be applied to make most patients have sufficient correlation. Whereas only 2 out of 10 subjects in both scans originally have correlation coefficients above 0.8, correcting the phase shift raises that number to 8 out of 10 subjects with enhanced correlations exceeding 0.8. Therefore, 80% of the subjects in this study possess respiratory patterns that are appropriate for respiratory gating. During simulation, the MPD and TCC methods can identify suitable subjects for respiratory-gated radiotherapy planning.

A clinical workflow for applying the phase-shift correction in an RGRT trial could follow the following seven steps: (1) simulate patient FB motion during the simulation 4DMRI scan and acquire concurrent external and internal waveforms, (2) assess the patient-specific phase shift and the degree of enhancement of the correlation between external and internal waveforms by correcting the phase shift, (3) select for RGRT planning only those patients whose enhanced correlation exceeds 0.9, (4) simulate bellows-triggered gating to select a beam-on threshold that minimizes the %harm by delivering radiation only within an acceptable motion margin (i.e., set a gating threshold at around 30% of the external surrogate's amplitude to achieve a motion margin of 50% or less of the internal target's amplitude), (5) use the simulated motion margin to design the patient's RGRT plan and devise a backup plan that accounts for the full-motion margin, (6) assess the correlation on the day of treatment by acquiring 20–30 s of fluoroscopic imaging to confirm the accuracy of the planned gating before initiating treatment, and (7) during treatment, radiographic imaging may be acquired periodically to verify the phase shift and check baseline to ensure accurate respiratory gating. Initially, it may take more effort to handle various clinical events and scenarios as any implementation of new procedures will. This motion assessment and management strategy could be useful for future MR-only RGRT simulation and planning and delivering the treatment using a conventional LINAC system.

Due to the differences between the shapes of the bellows and navigator waveforms, the efficiency of amplitude-triggered respiratory gating is relatively low (low duty cycle). Because the radiation beam may turn off too early, a large portion of the time that the navigator transits its motion margin goes unused. Further investigation—such as a deep-learning approach—may establish a patient-specific model that optimizes the accuracy and efficiency of respiratory gating.

In the future, strategies for enhancing the correlation between the motions of the diaphragm and a tumor and between the motions of the bellows and a tumor can also be investigated. It may then be possible to use the diaphragm as the internal surrogate for the motion of lung or liver tumors. With 20–30 s of fluoroscopic data and concurrent data acquired from an external surrogate, the patient's phase shift can be determined immediately before treatment and corrected—thereby ensuring enhanced correlation between the motions of an external surrogate and the tumor—throughout radiotherapy sessions lasting up to 30 min. The automatic motion-sampling tool can be readily applied to clinical applications. The correlation between the diaphragm and tumor can also be obtained during a simulation using TR-4DMRI. The strategy described herein for correcting the phase shift can readily be used to identify patients with severe breathing irregularities[53] who are unsuitable candidates for respiratory-gated radiotherapy.

## Conclusions

This study has demonstrated that the external–internal motion correlation can be significantly and stably enhanced to a high value (eg, r > 0.8) for 30 min of free-breathing by dynamically correcting a subject-specific phase shift. This result is supported by both the MPD and TCC methods. The subject-specific phase shifts tend to be stable over 30 min with small fluctuations, which can be well tolerated by the correlation-enhancement methods. Correcting the phase shift between an external surrogate and the internal target significantly improves the accuracy of amplitude-triggered respiratory gating, rendering correlation-based strategies safer and better equipped to guide radiotherapy.

### Ethical Statement

The human subject study is under an IRB-approved protocol (IRB 15-073, projects #4 and #6) and all participating subjects signed a written consent before entering the protocol study.

### Declaration of Conflicting Interests

The authors declared no potential conflicts of interest with respect to the research, authorship, and/or publication of this article.

## ORCID iD

Guang Li ![ORCID] https://orcid.org/0000-0002-9022-2883

## References

1. ICRU. Prescribing, recording, and reporting photon-beam intensity-modulated radiation therapy (IMRT) ICRU report 83. *J ICRU*. 2010;10:1–106.
2. Modh A, Rimner A, Williams E, et al. Local control and toxicity in a large cohort of central lung tumors treated with stereotactic body radiation therapy. *Int J Radiat Oncol Biol Phys*. 2014;90(5):1168–1176.
3. Yorke ED, Wang L, Rosenzweig KE, Mah D, Paoli JB, Chui CS. Evaluation of deep inspiration breath-hold lung treatment plans with Monte Carlo dose calculation. *Int J Radiat Oncol Biol Phys*. 2002;53(4):1058–1070.
4. Keall PJ, Mageras GS, Balter JM, et al. The management of respiratory motion in radiation oncology report of AAPM task group 76. *Med Phys*. 2006;33(10):3874–3900.
5. Shirato H, Onimaru R, Ishikawa M, et al. Real-time 4-D radiotherapy for lung cancer. *Cancer Sci.* 2012;103(1):1–6.
6. Li G, Mageras G, Dong L, Mohan R. Image-guided radiation therapy. In: Khan FM, Gerbi BJ, Sperduto PW, eds. *Treatment Planning in Radiation Oncology*. 4th Edition ed. Philadelphia, PA: Lippincott Williams & Wilkins; 2016:177–202.
7. Keall PJ, Colvill E, O'Brien R, et al. Electromagnetic-guided MLC tracking radiation therapy for prostate cancer patients: prospective clinical trial results. *Int J Radiat Oncol Biol Phys*. 2018;101(2):387–395.
8. Muacevic A, Drexler C, Wowra B, et al. Technical description, phantom accuracy, and clinical feasibility for single-session lung radiosurgery using robotic image-guided real-time respiratory tumor tracking. *Technol Cancer Res Treat*. 2007;6(4):321–328.
9. Chen VJ, Oermann E, Vahdat S, et al. Cyberknife with tumor tracking: an effective treatment for high-risk surgical patients with stage I non-small cell lung cancer. *Front Oncol*. 2012;2:9.
10. Poels K, Dhont J, Verellen D, et al. A comparison of two clinical correlation models used for real-time tumor tracking of semi-periodic motion: a focus on geometrical accuracy in lung and liver cancer patients. *Radiother Oncol*. 2015;115(3):419–424.
11. Zhang P, Hunt M, Telles AB, et al. Design and validation of a MV/kV imaging-based markerless tracking system for assessing real-time lung tumor motion. *Med Phys*. 2018;45(12):5555–5563.
12. Smith RL, Lechleiter K, Malinowski K, et al. Evaluation of linear accelerator gating with real-time electromagnetic tracking. *Int J Radiat Oncol Biol Phys*. 2009;74(3):920–927.
13. Kim T, Lewis BC, Price A, et al. Direct tumor visual feedback during free breathing in 0.35T MRgRT. *J Appl Clin Med Phys*. 2020;21(10):241–247.
14. Kim T, Lewis B, Lotey R, Barberi E, Green O. Clinical experience of MRI(4D) QUASAR motion phantom for latency measurements in 0.35T MR-LINAC. *J Appl Clin Med Phys*. 2021;22(1):128–136.

15. Jupitz SA, Shepard AJ, Hill PM, Bednarz BP. Investigation of tumor and vessel motion correlation in the liver. *J Appl Clin Med Phys*. 2020;21(8):183–190.
16. Low DA, Parikh PJ, Lu W, et al. Novel breathing motion model for radiotherapy. *Int J Radiat Oncol Biol Phys*. 2005;63(3):921–929.
17. Zhang Q, Pevsner A, Hertanto A, et al. A patient-specific respiratory model of anatomical motion for radiation treatment planning. *Med Phys*. 2007;34(12):4772–4781.
18. Li R, Lewis JH, Jia X, et al. On a PCA-based lung motion model. *Phys Med Biol*. 2011;56(18):6009–6030.
19. Al-Mayah A, Moseley J, Velec M, Brock KK. Sliding characteristic and material compressibility of human lung: parametric study and verification. *Med Phys*. 2009;36(10):4625–4633.
20. Ackerley EJ, Cavan AE, Wilson PL, Berbeco RI, Meyer J. Application of a spring-dashpot system to clinical lung tumor motion data. *Med Phys*. 2013;40(2):021713.
21. Yuan A, Wei J, Gaebler CP, Huang H, Olek D, Li G. A novel respiratory motion perturbation model adaptable to patient breathing irregularities. *Int J Radiat Oncol Biol Phys*. 2016;96(5):1087–1096.
22. Seregni M, Cerveri P, Riboldi M, Pella A, Baroni G. Robustness of external/internal correlation models for real-time tumor tracking to breathing motion variations. *Phys Med Biol*. 2012;57(21):7053–7074.
23. Li G, Wei J, Huang H, Gaebler CP, Yuan A, Deasy JO. Automatic assessment of average diaphragm motion trajectory from 4DCT images through machine learning. *Biomed Phys Eng Express*. 2015;1(4):045015.
24. Smith RL, Yang D, Lee A, Mayse ML, Low DA, Parikh PJ. The correlation of tissue motion within the lung: implications on fiducial based treatments. *Med Phys*. 2011;38(11):5992–5997.
25. Lin T, Li R, Tang X, Dy JG, Jiang SB. Markerless gating for lung cancer radiotherapy based on machine learning techniques. *Phys Med Biol*. 2009;54(6):1555–1563.
26. Berkels B, Bauer S, Ettl S, Arold O, Hornegger J, Rumpf M. Joint surface reconstruction and 4D deformation estimation from sparse data and prior knowledge for marker-less respiratory motion tracking. *Med Phys*. 2013;40(9):091703.
27. Mori S, Karube M, Shirai T, et al. Carbon-ion pencil beam scanning treatment with gated markerless tumor tracking: an analysis of positional accuracy. *Int J Radiat Oncol Biol Phys*. 2016;95(1):258–266.
28. Pepin EW, Wu H, Zhang Y, Lord B. Correlation and prediction uncertainties in the cyberknife synchrony respiratory tracking system. *Med Phys*. 2011;38(7):4036–4044.
29. Seppenwoolde Y, Shirato H, Kitamura K, et al. Precise and real-time measurement of 3D tumor motion in lung due to breathing and heartbeat, measured during radiotherapy. *Int J Radiat Oncol Biol Phys*. 2002;53(4):822–834.
30. Tsunashima Y, Sakae T, Shioyama Y, et al. Correlation between the respiratory waveform measured using a respiratory sensor and 3D tumor motion in gated radiotherapy. *Int J Radiat Oncol Biol Phys*. 2004;60(3):951–958.
31. Korreman SS, Juhler-Nottrup T, Boyer AL. Respiratory gated beam delivery cannot facilitate margin reduction, unless combined with respiratory correlated image guidance. *Radiother Oncol*. 2008;86(1):61–68.

32. Milewski AR, Olek D, Deasy JO, Rimner A, Li G. Enhancement of long-term external-internal correlation by phase-shift detection and correction based on concurrent external bellows and internal navigator signals. *Adv Radiat Oncol*. 2019;4(2):377–389.

33. Otani Y, Fukuda I, Tsukamoto N, et al. A comparison of the respiratory signals acquired by different respiratory monitoring systems used in respiratory gated radiotherapy. *Med Phys*. 2010;37(12):6178–6186.

34. Ge J, Santanam L, Yang D, Parikh PJ. Accuracy and consistency of respiratory gating in abdominal cancer patients. *Int J Radiat Oncol Biol Phys*. 2013;85(3):854–861.

35. Li G, Wei J, Olek D, et al. Direct comparison of respiration-correlated four-dimensional magnetic resonance imaging reconstructed using concurrent internal navigator and external bellows. *Int J Radiat Oncol Biol Phys*. 2017;97(3):596–605.

36. Li G, Wei J, Kadbi M, et al. Novel super-resolution approach to time-resolved volumetric 4-dimensional magnetic resonance imaging with high spatiotemporal resolution for multi-breathing cycle motion assessment. *Int J Radiat Oncol Biol Phys*. 2017;98(2):454–462.

37. Liu J, Lin T, Fan J, Chen L, Price R, Ma CC. Evaluation of the combined use of two different respiratory monitoring systems for 4D CT simulation and gated treatment. *J Appl Clin Med Phys*. 2018;19(5):666–675.

38. Li G, Arora NC, Xie H, et al. Quantitative prediction of respiratory tidal volume based on the external torso volume change: a potential volumetric surrogate. *Phys Med Biol*. 2009;54(7):1963–1978.

39. Mukumoto N, Nakamura M, Sawada A, et al. Accuracy verification of infrared marker-based dynamic tumor-tracking irradiation using the gimbaled x-ray head of the Vero4DRT (MHI-TM2000). *Med Phys*. 2013;40(4):041706.

40. Cai J, Chang Z, O'Daniel J, et al. Investigation of sliced body volume (SBV) as respiratory surrogate. *J Appl Clin Med Phys*. 2013;14(1):3987.

41. Seregni M, Kaderka R, Fattori G, et al. Tumor tracking based on correlation models in scanned ion beam therapy: an experimental study. *Phys Med Biol*. 2013;58(13):4659–4678.

42. Fassi A, Schaerer J, Fernandes M, Riboldi M, Sarrut D, Baroni G. Tumor tracking method based on a deformable 4D CT breathing motion model driven by an external surface surrogate. *Int J Radiat Oncol Biol Phys*. 2014;88(1):182–188.

43. Santoro JP, Yorke E, Goodman KA, Mageras GS. From phase-based to displacement-based gating: a software tool to facilitate respiration-gated radiation treatment. *J Appl Clin Med Phys*. 2009;10(4):132–141.

44. Lee M, Yoon K, Cho B, et al. Comparing phase- and amplitude-gated volumetric modulated arc therapy for stereotactic body radiation therapy using 3D printed lung phantom. *J Appl Clin Med Phys*. 2019;20(2):107–113.

45. Li G, Sun A, Nie X, et al. Introduction of a pseudo demons force to enhance deformation range for robust reconstruction of super-resolution time-resolved 4DMRI. *Med Phys*. 2018;45(11):5197–5207.

46. Nie X, Saleh Z, Kadbi M, et al. A super-resolution framework for the reconstruction of T2-weighted (T2w) time-resolved (TR) 4DMRI using T1w TR-4DMRI as the guidance. *Med Phys*. 2020;47(7):3091–3102.

47. Nie X, Huang K, Deasy J, Rimner A, Li G. Enhanced super-resolution reconstruction of T1w time-resolved 4DMRI in low-contrast tissue using 2-step hybrid deformable image registration. *J Appl Clin Med Phys*. 2020;21(10):25–39.

48. Li G, Huang H, Wei J, et al. Novel spirometry based on optical surface imaging. *Med Phys*. 2015;42(4):1690–1697.

49. Li G, Wei J, Huang H, et al. Characterization of optical-surface-imaging-based spirometry for respiratory surrogating in radiotherapy. *Med Phys*. 2016;43(3):1348–1360.

50. Cervino LI, Chao AK, Sandhu A, Jiang SB. The diaphragm as an anatomic surrogate for lung tumor motion. *Phys Med Biol*. 2009;54(11):3529–3541.

51. Cervino LI, Jiang Y, Sandhu A, Jiang SB. Tumor motion prediction with the diaphragm as a surrogate: a feasibility study. *Phys Med Biol*. 2010;55(9):N221–N229.

52. Yang J, Cai J, Wang H, et al. Is diaphragm motion a good surrogate for liver tumor motion? *Int J Radiat Oncol Biol Phys*. 2014;90(4):952–958.

53. Hindley N, Keall P, Booth J, Shieh CC. Real-time direct diaphragm tracking using kV imaging on a standard linear accelerator. *Med Phys*. 2019;46(10):4481–4489.

54. Meschini G, Paganelli C, Gianoli C, et al. A clustering approach to 4D MRI retrospective sorting for the investigation of different surrogates. *Phys Med*. 2019;58:107–113.